

## Evolution of secondary cellular circulation flow above submarine bedforms imaged by remote sensing techniques

I. Hennings<sup>(1)</sup>, D. Herbers<sup>(1)</sup>

1. GEOMAR Helmholtz-Zentrum für Ozeanforschung Kiel, Kiel, Germany -  
ihennings@geomar.de

### Abstract

Normalized radar cross section (NRCS) modulation and acoustic Doppler current profiler (ADCP) measurements above submarine sand ribbons and sand waves are presented. The two study areas are located in the Southern Bight of the North Sea at the *Birkenfels* wreck and in the sand wave field of the Lister Tief in the German Bight of the North Sea. These measurements reveal the developments of secondary cellular circulations in tidally induced coastal sea areas. Secondary circulation cells can develop perpendicular as well as parallel to the direction of the dominant tidal current flow. Circulation cells developed perpendicular to the direction of the dominant tidal current flow are associated with marine sand ribbons manifested near an underwater wreck. Secondary circulation cells within the water column observed parallel to the direction of the dominant tidal current flow have been initiated during flood and ebb tidal current phases associated with submarine sand waves. These two types of cellular circulations must obey the Hamiltonian principle of classical mechanics. The current–short surface wave interaction is described by the action balance or radiation balance-equation based on weak hydrodynamic interaction theory. The calculated current gradient or strain rate of the applied imaging theory has the same order of magnitude for both bedforms such as marine sand ribbons and sand waves, respectively.

### 1. INTRODUCTION

During the last three decades it turned out that the wave-current-bedform interaction mechanism is a rather complex process. Marine remote sensing data gave a certain impulse for the explanation of the different imaging mechanisms in the visible, infrared and microwave parts of the electromagnetic spectrum as well as in the sound waves spectrum. Normalized radar cross section (NRCS) modulation and acoustic Doppler current profiler (ADCP) measurements above submarine sand ribbons and sand waves reveal the development of secondary cellular circulation in tidally induced coastal sea areas. Mathematically and physically such kind of associated hydrodynamics obeys the Hamiltonian principle of classical mechanics (Neumann 1946, Neumann 1949, Alpers & Hasselmann 1978).

Secondary circulation cells can develop perpendicular as well as parallel to the direction of the dominant tidal current flow  $\mathbf{U}_0$ . In this paper both cases will be presented. Secondary circulation cells developed perpendicular to the direction of  $\mathbf{U}_0$  are associated with marine sand ribbons

manifested near an underwater wreck in the Southern Bight of the North Sea (Hennings & Herbers 2010). In contrast, secondary circulation cells related parallel to the dominant direction of the tidal flow  $\mathbf{U}_0$  are associated with marine sand waves in the tidal inlet of the Lister Tief in the German Bight of the North Sea (Hennings & Herbers 2006).

A similar kind of secondary circulation arising in the water is the vortex pair generated by the ship hull. Lateral current gradients behind the ship have been measured (Marmorino & Trump 1996). Surface strain rates associated with the divergent flow had a value of  $\partial u / \partial x = 0.03 \text{ s}^{-1}$ . This strain rate is of the same order of magnitude as strain rates associated with internal waves, fronts and sea bottom topography in littoral waters (Gasparovic & Apel 1988, Marmorino & Trump 1994, Hennings & Herbers 2010).

The motivation for this study is the mathematical and physical formulation of the imaging mechanism of radar signatures at the sea surface caused by submerged wrecks as well as ADCP measurements above marine sand waves. First, the

formation of wreck marks like sand ribbons at the sea bed and the associated manifestation of radar signatures at the water surface caused by a vortex pair or helical flow cells triggered by unidirectional tidal current flow interacting with a wreck are summarized. Second, the ADCP measurements and the characteristic flow related to marine sand waves in a tidal channel are shown. In section 2, a brief background of the theory is presented. Secondary circulation flow associated with sand ribbons and sand waves are described in section 3. Finally, section 4 contains the discussion and conclusions.

## 2. THEORY

The equations of Hamiltonian flow in phase space connect position  $x$  with momentum  $p_x$  through the Hamiltonian  $H$ . Volume in phase space is conserved under Hamiltonian flow, a property known today as Liouville's theorem (Nolte 2010). Neumann (1946) already concluded that a cellular current must obey the Hamiltonian principle of classical mechanics. The so called standing cellular wave published by Neumann (1946) is shown in Figure 1. Standing cellular circulation implies that volume or mass is not only be conserved by an acceleration or deceleration of the flow associated with submarine bedforms but that up- and downwelling of the three-dimensional current field is also important (see section 3). According to this fundamental background the current-short surface wave interaction can be described by the action balance or radiation balance equation (Alpers & Hasselmann 1978)

$$\frac{dN}{dt} = \left( \frac{\partial}{\partial t} + \dot{\mathbf{x}} \frac{\partial}{\partial \mathbf{x}} + \dot{\mathbf{k}} \frac{\partial}{\partial \mathbf{k}} \right) N = \quad (1)$$

$S(\mathbf{x}, \mathbf{k}, t)$

where  $N$  is the wave action density spectrum,  $\mathbf{x}$  is the space variable,  $t$  is the time variable,  $\mathbf{k}$  is the wave number and  $S(\mathbf{x}, \mathbf{k}, t)$  is a source function. The waves propagate along trajectories in phase space which are given by the ray equations

$$\dot{\mathbf{x}} = \frac{\partial \omega}{\partial \mathbf{k}} \quad (2a)$$

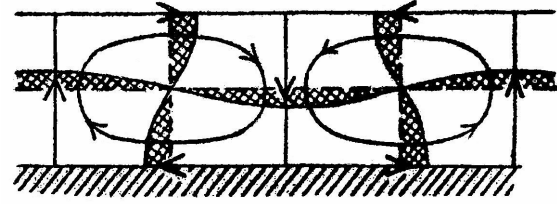


Figure 1. Standing cellular wave dynamics published by Neumann (1946).

$$\dot{\mathbf{k}} = \frac{\partial \omega}{\partial \mathbf{x}} \quad (2b)$$

where

$$\omega(\mathbf{x}, \mathbf{k}, t) = \omega'(\mathbf{k}) + \mathbf{k} \cdot \mathbf{U}(\mathbf{x}, t) \quad (3)$$

denotes the angular wave frequency in the moving medium with variable velocity  $\mathbf{U}(\mathbf{x}, t)$  and  $\omega'(\mathbf{k})$  is the intrinsic angular wave frequency.

The relationship between the wave height spectrum  $\Psi(\mathbf{k})$ , the wave-energy density spectrum  $F(\mathbf{k})$  and the wave action density spectrum  $N(\mathbf{k}) = F(\mathbf{k})(\omega'(\mathbf{k}))^{-1}$  is defined by (Holliday et al. 1986)

$$F(\mathbf{k}) = \omega'(k)N(\mathbf{k}) = \frac{\omega'(k)^2}{k} \psi(\mathbf{k}) \quad (4)$$

After transforming the mathematical formulations like described by Alpers & Hennings (1984) have been carried out then the expression for the modulation of the first order perturbed wave energy density spectrum  $\delta F/F_0 = (F - F_0)/F_0$ , with  $F_0$  as the unperturbed and  $F$  as the local wave energy density spectrum, respectively, is derived as a first approximation

$$\frac{\delta F}{F_0} = - (4 + \gamma) \frac{\partial u_{\text{perp}}}{\partial x_{\text{perp}}} \left( \left( \mathbf{c}_g + \mathbf{U}_0 \right) \frac{1}{L} + \mu \right)^{-1} \quad (5)$$

where  $\gamma$  is the relation between the group velocity  $\mathbf{c}_g$  and the phase velocity of the short waves,  $\partial u_{\text{perp}} / \partial x_{\text{perp}}$  is the gradient or strain rate of the current velocity component of the secondary circulation perpendicular to the bedform,  $\mathbf{U}_0$  is the mean dominant tidal current flow of the undisturbed sea area,  $L$  denotes the spatial scale of the flow cell in  $x_{\text{perp}}$ -direction, and  $\mu$  is the relaxation rate parameter. Equation (5) describes that the modulation of the first-order perturbed wave energy density spectrum of capillary and short gravity waves is proportional to the current

gradient of the secondary circulation caused by marine bedforms such as sand ribbons (Kenyon 1970) and sand waves (Hennings & Herbers 2010). However, equation (5) is only valid if the one-dimensional model for describing the sea bottom topography-current interaction is applicable. Otherwise, a full three-dimensional approach is required. If it is assumed that the radar is a linear imaging system then the relative radar image intensity modulation  $\delta I/I_0$  is equal to the relative normalized radar cross section (NRCS) modulation  $\delta\sigma/\sigma_0$  based on quasi-specular scattering. It follows that  $\delta\sigma/\sigma_0$  is then proportional to  $\delta F/F_0$  defined in equation (5) (Hennings & Herbers 2010).

### 3. SECONDARY CIRCULATION

Transverse secondary circulation of flow over a rough sea bed is equivalent to Langmuir circulation at the water surface due to wind stress. Circulation patterns associated with Langmuir super cells off the coast of New Jersey of the eastern U.S. coast have been identified by Gargett et al. (2004). The dominant scale of such circulation may be responsible for low-relief sand ribbons in the presence of strong tidal currents. Karl (1980) and Viekman et al. (1992) assumed that helical secondary-flow circulation within a boundary layer is responsible for the lineation development of sand ribbons and sedimentary furrows. Secondary circulations in the sea bottom boundary layer concentrate large, low-density particles in zones where there is flow convergence on the sediment surface. Thereupon, lineations such as sand ribbons can be formed. The schematic representation of the relationship between secondary circulations in the boundary layer, zones of convergence and divergence on the sea bed, sand ribbons, and sedimentary furrows in the model of furrow maintenance is presented in Figure 2 (Viekman et al. 1992). Hulscher (1996) shows that inclusion of vertical flow structures turned out to be necessary to describe the formation, or absence, of all known large-scale regular sea bottom features. The residual component of the vertical velocity is one order of magnitude smaller than the horizontal residual

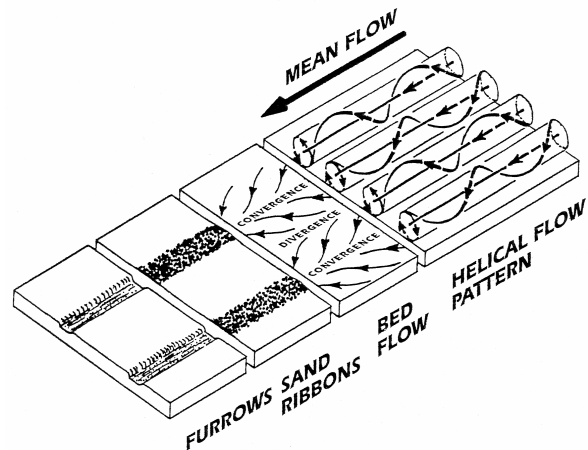


Figure 2. Schematic representation of the relationship between secondary circulations of the boundary layer, zones of convergence and divergence on the sea bed, sand ribbons, and sedimentary furrows in the model of furrow maintenance according to Viekman et al. (1992). Copyright 1992 by the American Society of Limnology and Oceanography, Inc.

velocity. It is directed upward above the crests and downward towards the troughs. These residual flow components cause a residual circulation which favours the growth of the bedform, as outlined in Fig. 2. In situ measurements verify up- and downwelling phenomena of the three-dimensional current velocity field contributing significantly to the interaction between marine sand waves and the tidal flow, which has not been known before in detail (see section 3.2, Alpers & Hennings 2004, Hennings and Herbers 2006). The up- and downwelling regimes cause remarkable depressions at the troughs of sand waves with a maximum depth of 2 m and a width of maximum 50 m (Hennings & Herbers 2006).

An elliptical vortex pair or elliptical helical flow cells are assumed as a first approximation to explain the interactions between the wreck mark, the (tidal) current, the residual flow and the water surface roughness. This assumption was based on the formation of wreck marks such as sand ribbons at the sea bed as shown in Fig. 2 and the manifestation of associated radar signature at the water surface as well as due to spatial considerations presented in section 3.1.

### 3.1 Sand ribbon associated with secondary circulation flow

The following relation can be derived for  $\partial u_{\text{perp}} / \partial x_{\text{perp}}$  from equation (5) according to Hennings & Herbers (2010):

$$\frac{\partial u_{\text{perp}}}{\partial x_{\text{perp}}} = \frac{u_{\text{perp}} \cdot z}{R} \left( 1 - 2 \frac{R^2}{z^2} \right) \times \left( \frac{x_{\text{perp}}}{R \cdot z} + (z_{\text{max}} - z) \cdot 2F_{sp} \cdot (x_{\text{perp}} - R)^2 \frac{1}{z^2} \right) \quad (6)$$

where  $R = |\mathbf{R}|$  of the space vector of a point on an ellipse in the Cartesian coordinate system,  $u_{\text{perp}}$  is the tangential current of an elliptical gyre at the sea surface in  $x_{\text{perp}}$ -direction,  $z$  is the water depth,  $z_{\text{max}}$  is the maximum water depth, and  $F_{sp}$  is the so-called shape parameter, which determines the slope of the sand ribbon.

Due to the analysed *Birkenfels* wreck data (Hennings & Herbers 2010) it turned out that only one of the two possible circulation cells downstream of the wreck is responsible for the manifestation of the radar signature (see also Fig. 3). Otherwise the bright and dark signatures as well as the spatial scales of  $\delta I/I_0$  are not consistent with the theoretical assumptions. The reason for the manifestation of only one bright as well as one dark radar signature can be due to the following effect: The inactive circulation cell has been not developed to such an extent that the current gradients become too weak to produce a significant NRCS modulation. This can happen due to changing tidal current directions of  $\mathbf{U}_0$  relative to the orientation of the wreck and sand ribbon, which has been indeed observed above marine sand waves (Hennings et al. 2000). However, Innes McCartney, a wreck specialist, reported in *Divernet*, the *Diver Magazine Online* (2012), that strong tidal currents can be developed at a wreck even in a water depth of 70 m lying in the sea area between the island of Alderney and Cape Le Hague in the English Channel. McCartney discovered the wreck on 4 July 2006 off Cape Le Hague which was the German Navy raider *Komet*. The *Komet* sunk on 14 October 1942. In 2007 it took two days for the divers to work out how to negotiate the treacherous currents in the area. The currents run fiercely over the upturned hull. But the uncertainty over the true nature of the water motion around a wreck underlines just how valuable in situ current

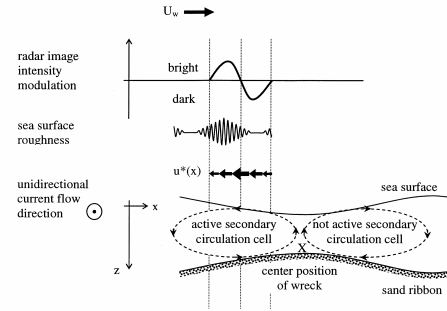


Figure 3. Schematic sketch of the unidirectional ebb tidal current flow (direction coming out of the graphic plane), cross-structure secondary circulation cells above sand waves or sand ribbons, centre position of wreck, marked by the capital letter X, sea surface, horizontal component of the tangential current of the secondary circulation cell  $u^* = u_{\text{perp}}$  in  $x = x_{\text{perp}}$ -direction at the sea surface, associated sea surface roughness and radar image intensity modulation due to accelerated and decelerated sea surface current velocities of the active secondary circulation cell. The wind direction  $U_w$  is indicated by an arrow and the left and right vertical lines indicate schematically the space range of 200 m used for simulations.

measurements would have been in this situation. On the basis of these considerations, Figure 3 presents a schematic view of the radar imaging mechanism of the submerged *Birkenfels* wreck and the associated sand ribbon. More details are described in Fig. 3's caption.

The comparison of simulated and measured NRCS modulation as a function of position is shown in Figure 4d. The simulated water depth as a function of position ( $-100 \text{ m} \leq x = x_{\text{perp}} \leq 100 \text{ m}$ ) with a total length of  $x_{\text{perp}} = 200 \text{ m}$  is presented in Figure 4a and has been used for all simulations. Figure 4b shows the simulated perpendicular current speed  $u_{\text{perp}} = u^*$  relative to  $\mathbf{U}_0$ . A maximum current speed of  $u_{\text{perp}}^{\text{max}} = -0.34 \text{ m s}^{-1}$  has been calculated. The strain rate or the gradient of the perpendicular component relative to  $\mathbf{U}_0$  of the current velocity  $\partial u_{\text{perp}} / \partial x_{\text{perp}}$  is presented in Figure 4c. Minimum and maximum strain rates varied between  $-0.0084 \text{ s}^{-1}$  and  $0.0088 \text{ s}^{-1}$ . The comparison of simulated NRCS modulation  $(\delta\sigma/\sigma_0)_{\text{sim}}$  and measured NRCS modulation  $(\delta\sigma/\sigma_0)_{\text{meas}}$  as a function of position is shown in Figure 4d. The calculations for  $(\delta\sigma/\sigma_0)_{\text{sim}}$

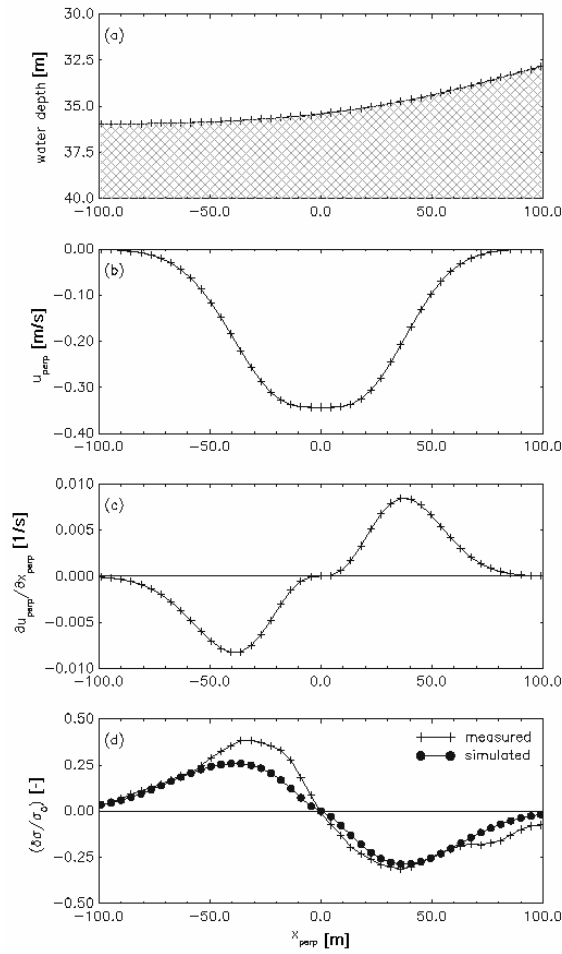


Figure 4. Results of simulations according to Hennings & Herbers (2010): (a) water depth as a function of  $x_{\text{perp}}$ , (b) perpendicular current speed  $u_{\text{perp}}$  relative to  $\mathbf{U}_0$ , (c) strain rate or gradient of the perpendicular component relative to  $\mathbf{U}_0$  of the current velocity  $\partial u_{\text{perp}} / \partial x_{\text{perp}}$ , (d) comparison of simulated  $(\delta\sigma/\sigma_0)_{\text{sim}}$  and measured  $(\delta\sigma/\sigma_0)_{\text{meas}}$  NRCS modulation.

applying equations (1)-(26) from Hennings & Herbers (2010) have been carried out for  $\theta_0 = 70^\circ$ ,  $g = 9.81 \text{ m s}^{-2}$ ,  $\rho = 1026 \text{ kg m}^{-3}$ ,  $T = 73 \times 10^{-6} \text{ m}^3 \text{ s}^{-2}$ ,  $B = 4.6 \times 10^{-3}$ ,  $B' = 3.15 \times 10^{-2}$ ,  $k_v = 502.28 \text{ m}^{-1}$ ,  $U_0 = 0.8 \text{ m s}^{-1}$ ,  $U_w = 9 \text{ m s}^{-1}$ ,  $L = 369 \text{ m}$ ,  $\mu = 1 \text{ s}^{-1}$ ,  $a = 184.50 \text{ m}$ ,  $b = 25.04 \text{ m}$ ,  $h_0 = 5 \text{ m}$ , and  $z_{\text{max}} = 36 \text{ m}$ . The value for  $\mu$  is in the range of parameterizations for the  $K_a$  band radar as published by Caponi et al. (1988). The direction of  $\mathbf{c}_g$  has been assumed equal to the wind direction from  $270^\circ$ . For all simulations the perpendicular component of  $\mathbf{c}_g$  relative to  $\mathbf{U}_0$  in the direction of  $x_{\text{perp}}$  has been used. The simulated NRCS modulation  $(\delta\sigma/\sigma_0)_{\text{sim}}$  presented in Figure 4d shows

a maximum modulation  $(\delta\sigma/\sigma_0)_{\text{sim}}^{\text{max}} = 0.26$  at the minimum strain rate (see Fig. 4c) and the measured maximum NRCS modulation  $(\delta\sigma/\sigma_0)_{\text{meas}}^{\text{max}} = 0.38$  is located also at the minimum strain rate. The measured minimum modulation  $(\delta\sigma/\sigma_0)_{\text{meas}}^{\text{min}} = -0.31$  at the maximum strain rate position agrees fairly well with the simulated modulation  $(\delta\sigma/\sigma_0)_{\text{sim}}^{\text{min}} = -0.29$  with a coinciding phase relation. The results of  $(\delta\sigma/\sigma_0)_{\text{sim}}$  presented in Figure 4d show the best fit to  $(\delta\sigma/\sigma_0)_{\text{meas}}$  based on available in situ data and most consistent other parameters like  $\mu$ .

### 3.2 Sand wave associated with secondary flow

The vertical flow components  $u_{\text{vert}}$  of the three-dimensional current field measured by the ADCP over asymmetric marine sand waves on the sea bottom in the study area of the Lister Tief in the German Bight of the North Sea are shown in Figures 5a-b at the end of the paper (Hennings & Herbers 2006). The current field has been measured by the ADCP of the same kind during ebb and flood tidal current phases, respectively. During flood tidal current phase the vertical component of the tidal current is reversed compared to the ebb tidal current phase. Upwelling events during ebb tidal current phase are associated with steep flanks of sand waves and during flood tidal current phase  $u_{\text{vert}}$  is related to downwelling events at the steep flanks of sand waves. The water depth dependent vertical component  $u_{\text{vert}}$  of the current velocity as a function of the horizontal space component perpendicular to the sand wave crest  $x_{\text{perp}}$  is shown in Fig. 5a and varies between  $-12 \text{ cm s}^{-1} \leq u_{\text{vert}} \leq 16 \text{ cm s}^{-1}$  during ebb tidal current phase at 0502-0513 UT on 10 August 2002. Last high water at station List was at 0243 UT on 10 August 2002. The downward orientated vertical component (dark or blue colour) is located at the troughs and gentle slopes of the sand waves. A regular structure of circulation cells of  $u_{\text{vert}}$  within the water column has been developed during that time of the ebb tidal current phase. The upward orientated vertical component  $u_{\text{vert}}$  of the current velocity (bright or yellow/red colour) has been developed at the steep flanks of sand waves and is superimposed on the divergent zones of the perpendicular component relative to the sand wave crest of the current velocity gradient  $\partial u_{\text{perp}} / \partial x_{\text{perp}}$ .

During flood tidal current phase at 1025-1031 UT on 10 August 2002  $u_{vert}$  varies between  $-16 \text{ cm s}^{-1} \leq u_{vert} \leq 12 \text{ cm s}^{-1}$  (Fig. 5b). Last low water at station List was at 0829 UT on 10 August 2002. The downward orientated vertical component (dark or blue colour) is located at the troughs and steep slopes of the sand waves and is superimposed on the convergent zones of the perpendicular component relative to the sand wave crest of the current velocity gradient  $\partial u_{perp}/\partial x_{perp}$ . The upward orientated vertical component (bright or yellow/red colour) is associated with the gentle slopes of the sand waves. These observations confirm the theory of the radar imaging mechanism of sea bottom topography presented by Alpers & Hennings (1984).

#### 4. CONCLUSIONS

The standing cellular wave mechanism published by Neumann (1946) has been visualized by the up- and downward orientated components  $u_{vert}$  of the three-dimensional current velocity field measured by the ADCP at stoss faces of asymmetric marine sand waves in the study area of the Lister Tief in the German Bight of the North Sea (Hennings et al. 2004). The so called “waterspouts” have been measured by the ADCP of the same kind during ebb and flood tidal current phases, respectively. During ebb tidal current phase the waterspouts are upwelling events and during flood tidal current phase they are associated with downwelling at the steep flanks of the investigated marine sand waves. It has to be noticed here, that observed vertical velocities over two-dimensional (2-D) dunes in a laboratory channel analyzed by Bennett & Best (1995) are directed downwards above the dune trough and upwards over the stoss during flood tidal phase. The vertical velocities described here have a different phase relationship to the sand waves.

The presented theory is a first-order theory, describing the NRCS modulation in the capillary as well as in the gravity wave ranges of the wave energy density spectrum due to secondary flow circulation or helical eddies caused by the investigated submerged wreck/sand ribbon configuration. The theoretical model proposed in this study is not able to explain all aspects of the NRCS modulation due to submerged wrecks

associated with sand ribbons in coastal waters. However, the quasi-specular scattering theory does produce sensible results at this stage in our understanding and can explain certain aspects of the radar signature. This subject has been shown by simulations of the NRCS modulation and by comparison with measured NRCS modulation data caused by the *Birkenfels* wreck of the southern North Sea (Hennings & Herbers 2010). That the quasi-specular theory is capable to explain the radar signature of the wreck/sand ribbon may be due to the fact that the *Birkenfels* wreck is lying more or less sub-parallel to the dominant regional tidal current direction.

From the results derived in this paper the following conclusions can be drawn for the NRCS modulation and ADCP measurements above submarine sand ribbons and sand waves revealing the developments of secondary cellular circulations in tidally induced coastal sea areas:

1. Wreck marks like sand ribbons as well as radar signatures of wrecks are indicators of local (tidal) current directions. Radar image signatures of wrecks associated with sand ribbons are indicators of secondary flow regimes or helical circulation cells triggered by unidirectional (tidal) current flow caused by submerged wrecks.
2. The simulated NRCS modulation  $(\delta\sigma/\sigma_0)_{sim}$  and the measured NRCS modulation  $(\delta\sigma/\sigma_0)_{meas}$  above the wreck/sand ribbon have the same order of magnitude with a coinciding phase relation. The difference between the maximum simulated and measured NRCS modulation is less than 31.6% and the difference between the minimum simulated and measured NRCS modulation is less than 6.5%. These results are acceptable but need to be improved.
3. The existence of a significant upward orientated vertical component  $u_{vert}$  of the three-dimensional current velocity field measured by the ADCP has been recorded. Marked waterspouts of  $u_{vert}$  have been measured in a more or less straight line in the vicinity of crests above steep slopes of flood tide oriented marine sand waves. These waterspouts created by  $u_{vert}$  produce upwelled water and create turbulence patterns at the water surface. The upward orientated patterns of  $u_{vert}$  are simultaneously superimposed on the divergent flow zones of  $\partial u_{perp}/\partial x_{perp}$ . The downward orientated vertical flow component of  $u_{vert}$  is located at the troughs and gentle slopes of the

marine sand waves. A regular structure of circulation cells of  $u_{vert}$  within the water column has been initiated during ebb tidal current phase. During flood tidal current phase the vertical component of the tidal current is reversed. This implies that mass is not only be conserved by an acceleration or deceleration of the flow in relation to marine sand waves. Up- and downwelling of the three dimensional current field also contribute significantly to the extensive circulation mechanism above marine sand waves in the study area of the Lister Tief.

## 5. REFERENCES

- Alpers, W. & Hasselmann, K. 1978. The two-frequency microwave technique for measuring ocean wave spectra from an airplane or satellite. *Boundary Layer Meteorology* 13: 215-230.
- Alpers, W. & Hennings, I. 1984. A theory of the imaging mechanism of underwater bottom topography by real and synthetic aperture radar. *Journal of Geophysical Research* 89(C6): 10529-10546.
- Bennett, S.J. & Best, J.L. 1995. Mean flow and turbulence structure over fixed, two-dimensional dunes: implications for sediment transport and bedform stability. *Sedimentology* 42: 491-513.
- Caponi, E.A., Crawford, D.R., Yuen, H.C. & Saffman, P.G. 1988. Modulation of radar backscatter from the ocean by a variable surface current. *Journal of Geophysical Research* 93(C6): 12249-12263.
- Gargett, A., Wells, J. Tejada-Martinez, A.E. & Grosch, C.E. 2004. Langmuir supercells: a mechanism for sediment resuspension and transport in shallow seas. *Science* 306: 1925-1928.
- Gasparovic, R.F. & Apel, J. 1988. An overview of the SAR internal wave signature experiment. *Journal of Geophysical Research* 93: 12304-12316.
- Hennings, I., Lurin, B., Vernemmen, C. & Vanhessche, U. 2000. On the behaviour of tidal current directions due to the presence of submarine sand waves. *Marine Geology* 169: 57-68.
- Hennings, I., Herbers, D., Prinz, K. & Ziemer, F. 2004. First results of the OROMA experiment in the Lister Tief of the German Bight in the North Sea. *EARSel eProceedings* 3: 86-104.
- Hennings, I. & Herbers, D. 2006. Radar imaging mechanism of marine sand waves at very low grazing angle illumination caused by unique hydrodynamic interactions. *Journal of Geophysical Research* 111: C10008, doi: 10.1029/2005JC003302.
- Hennings, I. & Herbers, D. 2010. A theory of the  $K_a$  band radar imaging mechanism of a submerged wreck and associated bed forms in the southern North Sea. *Journal of Geophysical Research* 115: C10047, doi: 10.1029/2010JC006360.
- Holliday, D., St-Cyr, G. & Woods, N.E. 1986. A radar ocean imaging model for small to moderate incidence angles. *International Journal of Remote Sensing* 7: 1809-1834.
- Hulscher, J.M.H. 1996. Tidal-induced large-scale regular bed form patterns in a three-dimensional shallow water model. *Journal of Geophysical Research* 101(C9): 20727-20744.
- Karl, H.A. 1980. Speculations on processes responsible for mesoscale current lineations on the continental shelf, southern California. *Marine Geology* 34: M9-M18.
- Kenyon, N.H. 1970. Sand ribbons of European tidal seas. *Marine Geology* 9: 25-39.
- Marmorino, G.O. & Trump, C.L. 1994. A salinity front and current rip near Cape Hatteras, North Carolina. *Journal of Geophysical Research* 99: 7627-7637.
- Marmorino, G.O. & Trump, C.L. 1996. Preliminary side-scan ADCP measurements across a ship's wake. *Journal of Atmospheric and Oceanic Technology* 13: 507-513.
- Neumann, G. 1946. Stehende zellulare Wellen im Meere. *Naturwissenschaften* 33: 282-283.
- Neumann, G. 1949. Stabilitätsschwingungen und die innere thermische Unruhe im Meer und in der Atmosphäre. *Deutsche Hydrographische Zeitschrift* 2: 52-67.
- Nolte, D.D. 2010. The tangled tale of phase space. *Physics Today* 63: 33-38.
- Viekman, B.E., Flood, R.D., Wimbush, M., Faghri, M., Asako, Y. & Van Leer, J.C. 1992. Sedimentary furrows and organized flow structure: A study in Lake Superior. *Limnology and Oceanography* 37: 797-812.

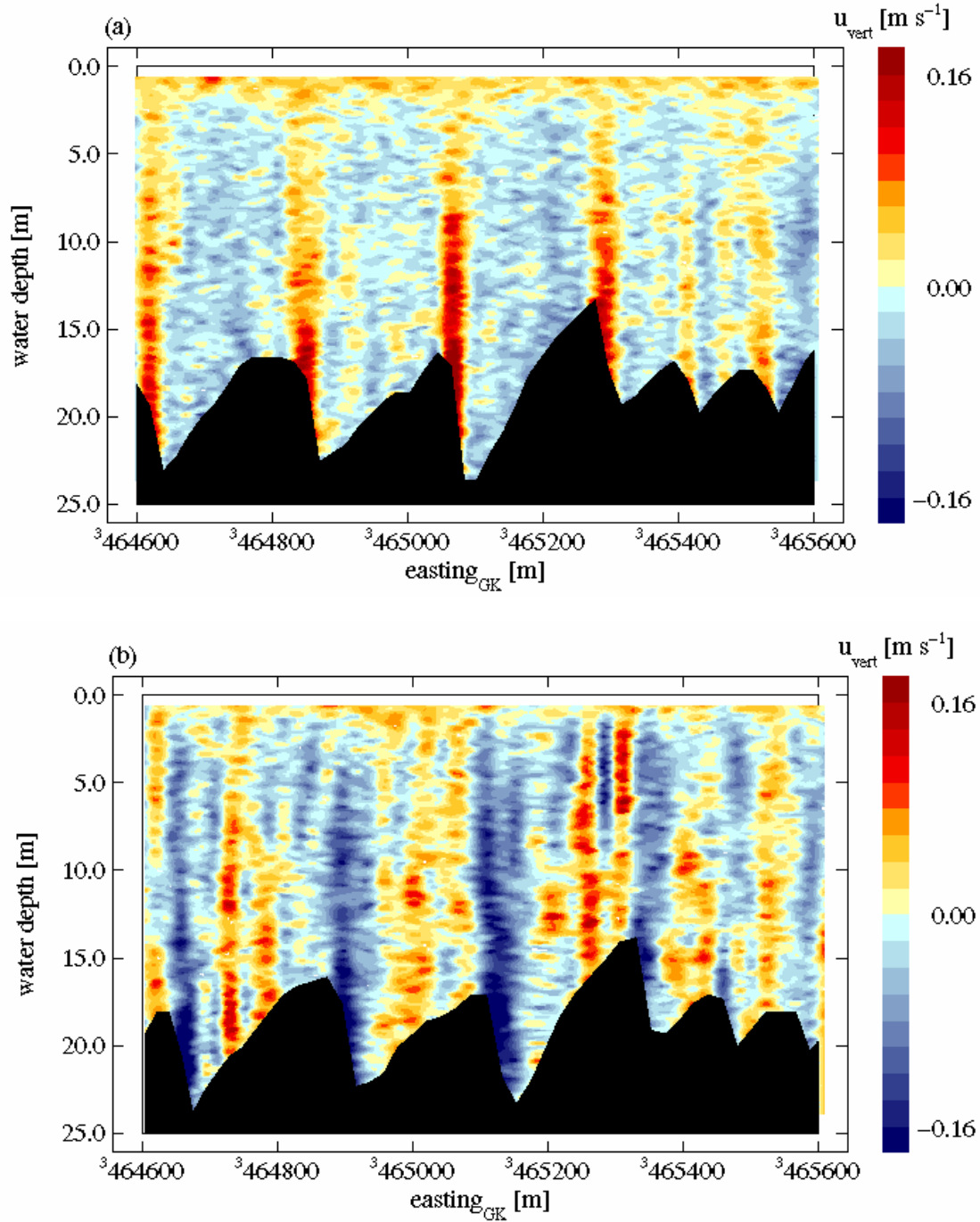


Figure 5. (a) Water depth dependent vertical component  $u_{\text{vert}}$  of the current velocity as a function of the horizontal space component perpendicular to the sand wave crest  $x_{\text{perp}}$ . The ADCP data from the near water surface to the sea bed have been obtained on board R.V. *Ludwig Prandtl* during ebb tidal current phase at 0502-0513 UT on 10 August 2002 along the profile AA' in the Lister Tief of the German Bight in the North Sea (Hennings & Herbers 2006). Dark or blue colour shows the downward and bright or yellow/red colour the upward orientated vertical component  $u_{\text{vert}}$ . The direction of the ebb tidal current is from right to left; (b) same as (a) but the data were measured during flood tidal current phase at 1025-1031 UT on 10 August 2002 along the profile AA'. The direction of the flood tidal current is from left to right.